



Irisin ameliorates doxorubicin-induced cardiac perivascular fibrosis through inhibiting endothelial-to-mesenchymal transition by regulating ROS accumulation and autophagy disorder in endothelial cells

Jian-an Pan^{a,1}, Hui Zhang^{a,b,1}, Hao Lin^a, Lin Gao^a, Hui-li Zhang^a, Jun-feng Zhang^{a,***}, Chang-qian Wang^{a,**}, Jun Gu^{a,*}

^a Department of Cardiology, Shanghai Ninth People's Hospital, Shanghai Jiaotong University School of Medicine, Shanghai, People's Republic of China

^b Department of Echocardiography, Zhongshan Hospital, Fudan University, Shanghai, People's Republic of China

ARTICLE INFO

Keywords:

Doxorubicin-induced cardiotoxicity
Perivascular fibrosis
Endothelial-to-mesenchymal transition
Irisin
Reactive oxygen species
Autophagy

ABSTRACT

The dose-dependent toxicity to cardiomyocytes has been well recognized as a central characteristic of doxorubicin (DOX)-induced cardiotoxicity (DIC), however, the pathogenesis of DIC in the cardiac microenvironment remains elusive. Irisin is a new hormone-like myokine released into the circulation in response to exercise with distinct functions in regulating apoptosis, inflammation, and oxidative stress. Recent advances revealed the role of irisin as a novel therapeutic method and an important mediator of the beneficial effects of exercise in cardioprotection. Here, by using a low-dose long-term mouse DIC model, we found that the perivascular fibrosis was involved in its myocardial toxicity with the underlying mechanism of endothelial-to-mesenchymal transition (EndMT). Irisin treatment could partially reverse DOX-induced perivascular fibrosis and cardiotoxicity compared to endurance exercise. Mechanistically, DOX stimulation led to excessive accumulation of ROS, which activated the NF- κ B-Snail pathway and resulted in EndMT. Besides, dysregulation of autophagy was also found in DOX-treated endothelial cells. Restoring autophagy flux could ameliorate EndMT and eliminate ROS. Irisin treatment significantly alleviated ROS accumulation, autophagy disorder, NF- κ B-Snail pathway activation as well as the phenotype of EndMT by targeting uncoupling protein 2 (UCP2). Our results also initially found that irisin was mainly secreted by cardiomyocytes in the cardiac microenvironment, which was significantly reduced by DOX intervention, and had a protective effect on endothelial cells in a paracrine manner. In summary, our study indicated that DOX-induced ROS accumulation and autophagy disorders caused an EndMT in CMECs, which played a role in the perivascular fibrosis of DIC. Irisin treatment could partially reverse this phenomenon by regulating UCP2. Cardiomyocytes were the main source of irisin in the cardiac microenvironment. The current study provides a novel perspective elucidating the pathogenesis and the potential treatment of DIC.

1. Introduction

Doxorubicin (DOX), one of the anthracycline compounds, is widely used in chemotherapy regimens [1]. But it is still the major culprit in chemotherapy-induced cardiotoxicity, which greatly limits its clinical application [2,3]. Previous studies about DOX-induced cardiotoxicity (DIC) mainly focused on the dose-dependent toxicity to cardiomyocytes with the hypothesis of the generation of excess reactive oxygen species

(ROS) and the inhibition of topoisomerase 2 β [3]. However, the heart is composed of about 30% of cardiomyocytes, and about 70% of non-cardiomyocytes. Recently, other cell types, such as endothelial cells (ECs), fibroblasts, and cardiac progenitor cells, have been proposed as additional targets, suggesting that the cardiotoxicity caused by DOX is closely related to the overall cardiac microenvironment and adding the complexity to explain the pathogenesis of DIC [4].

Previous reports demonstrated late cardiac remodeling with cardiac

* Corresponding author. No. 639 Zhizaoju Road, 200011, Shanghai, People's Republic of China.

** Corresponding author. No. 639 Zhizaoju Road, 200011, Shanghai, People's Republic of China.

*** Corresponding author. No. 639 Zhizaoju Road, 200011, Shanghai, People's Republic of China.

E-mail addresses: jfzhang_dr@163.com (J.-f. Zhang), wqian@hotmail.com (C.-q. Wang), gjforsub@163.com (J. Gu).

¹ These authors contributed equally to this work.

<https://doi.org/10.1016/j.redox.2021.102120>

Received 22 July 2021; Received in revised form 17 August 2021; Accepted 27 August 2021

Available online 31 August 2021

2213-2317/© 2021 The Authors.

Published by Elsevier B.V. This is an open access article under the CC BY-NC-ND license

(<http://creativecommons.org/licenses/by-nc-nd/4.0/>).

fibrosis following DOX treatment [5]. But a recent study found that the process of DOX-induced fibroblast activation and perivascular fibrosis were earlier than its myocardial toxicity [6]. ECs have been suggested to represent a source of cardiac fibroblasts by the program of endothelial-to-mesenchymal transition (EndMT), contributing to the pathogenesis of perivascular fibrosis [7]. EndMT, just like epithelial-mesenchymal transition (EMT), is a phenotypic switching process by which ECs lose their characteristics and acquire mesenchymal traits, which leads to endothelial dysfunction and interstitial fibrosis. The traditional mechanisms of EndMT mainly involved the upregulating of TGF- β /Smads, Notch, or Wnt/ β -catenin pathway and subsequent activation of transcription factors, such as Snail, Slug, and Twist [8]. A potential link between oxidative stress and EndMT has risen recently [9,10]. And numerous studies have implied that the increased ROS production played a central role in doxorubicin-mediated ECs toxicity [11]. However, the role of ROS-induced EndMT in perivascular fibrosis caused by DOX is still unclear.

Autophagy is a highly conserved catabolic process that mediates the degradation of pernicious or dysfunctional cellular components. Previous studies have shown that there is a certain degree of autophagy disorder in the process of DIC [12,13]. In addition, there is a complex relationship between autophagy-correlated and EMT-correlated signaling pathways [14]. Autophagy activation could suppress ROS-NF- κ B signaling [15] and promote Snail degradation [16,17], contributing to EMT or EndMT inhibition.

To date, there is no definitive treatment indicated to prevent or reverse DIC [2]. Although the heart failure medications such as β -blockers and angiotensin II inhibitors were used to relieve symptoms, none of them significantly improve the long-term prognosis [2]. Recent studies have shown that endurance exercise (EXE) is a non-pharmacological therapy that promises to attenuate DOX-induced cardiotoxicity [18]. But it is not generally used in cancer patients. Irisin is a new hormone-like myokine released into the circulation by cleavage of fibronectin type III domain-containing protein 5 (FNDC5) [19] and is significantly upregulated in response to EXE. Studies have reported that irisin antagonized the oxidative stress of cardiomyocytes in DIC [20]. Recently, some of its pleiotropic and favorable properties have been attributed to autophagy induction, posing irisin as an important regulator of autophagy by exercise [21]. Further, studies have proposed the endothelial protective effect of irisin in atherosclerosis and diabetic cardiomyopathy [22].

The aforementioned findings suggested that irisin could be a novel therapeutic method and an important mediator of the beneficial effects of exercise in cardioprotection. Here, to determine whether irisin influences DOX-induced perivascular fibrosis in the early stage, we investigated the precise effect of irisin on doxorubicin-induced EndMT in vitro and the function of irisin in DIC in vivo.

2. Materials and methods

2.1. Animal experiments

The study was ethically conducted in strict accordance with the recommendations of the "Guide for the Care and Use of Laboratory Animals published by the US NIH (NIH publication No. 85-23, revised 2011)" and approved by the Animal Experiment Ethics Committee of Shanghai ninth people's hospital. Male 5-wk-old C57BL/6J mice weighing 18–22 g were purchased from Shanghai Slac Experimental Animal Centre (Shanghai, China) and kept in sterilized filter top cages with controlled humidity and a 12-h day/night cycle at 22 °C. After 1 wk of the acclimation period, the animals were randomly divided into four groups (n = 10 per group): vehicle-treated group (Vehicle), DOX-treated group (DOX), DOX-treated plus EXE training group (DOX + EXE), and DOX plus irisin-treated group (DOX + Irisin). Mice were given DOX (i.p. 5 mg/kg; MedChem Express, USA) or an equivalent volume of the vehicle once a week for 4 weeks. Mice assigned to DOX + EXE group

performed treadmill running (13 m/min with 0% grade for 60 min/d, 5 d/wk) [23] 2 wk before and during DOX treated. Mice assigned to the DOX + Irisin group were treated with recombinant irisin (i.p. 1 mg/kg/d, 5 d/wk; Cayman Chemical, USA) 2 wk before and during DOX treatment. To inhibit the secretion of irisin in the myocardium, mice received a single intravenous injection of an adeno-associated serotype 9 (AAV9-U6-shRNA-CMV-GFP) viral vector expressing carrying mouse FNDC5 shRNA (AAV9-shFNDC5) or negative control (AAV9-NC) (Genomeditech, China) via the tail vein at a concentration of 1×10^{11} viral genome per mouse 4 wk before DOX injection. 2 wk after the last injection of DOX, echocardiography was implemented and ventricular tissues were obtained from mice euthanized using deep isoflurane (5%) anesthesia, rinsed in ice-cold phosphate buffer saline, and snap-frozen in liquid nitrogen. The experimental design paradigm was shown in Figs. S1A and S7A.

2.2. Echocardiography

Transthoracic echocardiography was performed through the UBM system (Vevo 2100, VisualSonics, Canada). Mice were anesthetized and maintained under 1–3% isoflurane during the procedure. Echocardiographic measurements were performed by a blinded investigator and were conducted at the mid-papillary muscle level, as guided by two-dimensional long-axis images. Fractional shortening and ejection fraction were measured and calculated with Vevo Analysis software.

2.3. Histologic evaluation

For the Hematoxylin-Eosin (HE) and Masson trichrome staining, the heart slides were deparaffinized and rehydrated by gradient elution using xylene and ethanol, and then were stained by hematoxylin-eosin (Solarbio, China) and Masson trichrome staining reagent (Solarbio, China) according to the manufacturer's instructions.

2.4. Isolation, culture, and identification of cardiomyocytes (CMs), cardiac fibroblasts (CFs), and cardiac microvascular endothelial cells (CMECs)

For CMs and CFs, the newborn C57BL/6J mice (within 36 h) were euthanized by decapitation and the hearts were collected and washed with pre-cooled phosphate-buffered saline (PBS). The tissues were cut into 1 mm^3 and subjected to digestive juice containing 0.25% pancreatic enzymes (Gibco, USA) and 0.025% type IV collagenase (Invitrogen, USA) for incubation at 37 °C for 5 min. The supernatant was then collected and transferred to Dulbecco's modified Eagle's medium (DMEM) (Hyclone, USA) supplemented with 10% fetal bovine serum (FBS) (Gibco, USA) to terminate the detachment. The tissue residue was digested 10 more times as above. All solutions were collected for centrifugation at 1000 rpm for 5 min and the deposit was resuspended with DMEM containing 10% FBS and 1% penicillin-streptomycin solution (P/S) (Hyclone, USA). After filtering through a 100- μ m mesh filter, the cell suspension was inoculated into culture dishes and cultured at 37 °C in a humidified incubator containing 95% air and 5% CO₂ for 1 h. The adherent CFs were identified by immunofluorescence of Vimentin. The upper cell suspension was collected and inoculated into new culture dishes pretreated with fibrous collagen (Sigma, USA) for 2d and the adherent CMs were identified by immunofluorescence of cTnT.

For CMECs, male 8-wk-old C57BL/6J mice were anesthetized using deep isoflurane (5%) anesthesia and the hearts were excised and rinsed with PBS supplemented with heparin. The left ventricle was dissected and immersed in 75% ethanol for 30 s to devitalize the epicardial mesothelial cells and endocardial endothelial cells. The remaining tissues were then cut into 1 mm^3 and subjected to digestive juice as above. Dissociated cells were filtered and centrifuged at 1000 rpm for 5 min. The cells were resuspended in ECM complete medium (ScienCell, USA) containing 5% FBS, 1% endothelial cell growth supplement (ECGS), and

1% P/S and then plated on fibrous collagen treated dishes. Primary cultures of CMECs were identified by immunofluorescence of CD31.

2.5. Cell treatment and transfection

The medium was refreshed every 3 days and replaced with serum-free DMEM for 12 h when cells were cultured at about 80% confluence. DOX treatment was used at different concentrations (0–5 μ M) for 48 h. For irisin treatment, cells were incubated with recombinant irisin (20 nM) for 48 h. For regulation of autophagy, cells were incubated with rapamycin (RAPA, 20 nM) (Selleck, USA) or 3-Methyladenine (3-MA, 5 mM) (Selleck, USA) for 48 h. For in vitro knockdown of UCP2 or FNDC5, a small interfering RNA (siRNA) molecule (siUCP2 or siFNDC5) (Genomeditech, China) was synthesized. The target sequences were listed in Tbl. S1. A random sequence molecule was synthesized as negative control respectively. Cells were seeded at a density of 1×10^5 cells/ml in a well plate containing growth medium without antibiotics and incubated overnight. Lipofectamin™ 3000 (Invitrogen, USA) was used according to the manufacturer's instructions for 48 h to transfect in OPTI-MEM reduced serum medium (Gibco, USA). The effects of these interventions were evaluated by real-time PCR. The following experimental treatments were performed after transfection.

2.6. RNA preparation and analysis

Total RNA was extracted from cells and cardiac tissues using the TRIzol reagent (Invitrogen, USA), and reverse-transcribed into cDNA using All-in-One cDNA Synthesis SuperMix (Bimake, USA). Next, the cDNA was quantitatively amplified using 2x SYBR Green qPCR Master Mix (Bimake, USA). Real-time PCR was conducted in triplicate using an Applied Biosystems 6Flex (ABI, USA). The sequences of the forward and reverse primers used for amplification are shown in Tbl. S2. The results were presented relative to the expression of the GAPDH gene by the Delta-Delta Ct method.

2.7. Enzyme-linked immunosorbent assay (ELISA)

To detect the content of irisin in mouse serum, heart tissues, and cell supernatant, a commercially available enzyme-linked immunosorbent assay kit (EK-067-29; Phoenix Pharmaceuticals, USA) was used according to the manufacturer's instructions.

2.8. Tube formation assay

Matrigel (Corning, USA) was paved on a 24-well plate for solidification at 37 °C for 1 h. Treated CMECs were resuspended and seeded onto the matrigel plates at 1×10^5 cells/well in triplicate. The ring structures formatted by CMECs were monitored using an inverted microscope (Nikon, Japan) and photographed in three random fields after 8 h. Image analysis was carried out by Angiogenesis Analyze in image J software.

2.9. Wound healing assay and migration assay

For scratch wound healing assay, treated CMECs were scratched by 1 mL pipette tips and washed two times with PBS. Subsequently, the cells were cultured in ECM medium with 1% FBS for 24 h. The images were recorded with an inverted microscope (Nikon, Japan) at 0 and 24 h. For migration assay, a transwell system containing a polycarbonate filter with a pore size of 8.0 μ m (Corning, USA) was used. The lower chambers were filled with an 800 μ l ECM medium with 5% FBS. The treated CMECs were resuspended in 200 μ l of serum-free ECM medium and added to the upper chamber. After incubation for 24 h, the cells in the upper chamber were removed using a cotton tip and the cells migrated into the reverse side of the membrane were fixed and stained by 1% crystal violet (Beyotime Biotechnology, China). Five visual fields were

selected randomly under an inverted microscope (Nikon, Japan) and the wound gap areas and migrated cells were analyzed by Image J software.

2.10. Determination of autophagy flux

CMECs were seeded and transfected with pGMLV-GFP-LC3 Lenti-virus (Genomeditech, China) at 30 multiplicities of infection (MOI) for 24 h. Subsequently, cells were treated as mentioned above. After treatments, the GFP-LC3B fusion protein was visualized under a Nikon Eclipse Ti inverted fluorescence microscope (Nikon, Japan).

2.11. Measurement of intracellular ROS and mitochondrial ROS

Total ROS levels in CMECs were measured using the Fluorometric Intracellular ROS Kit (MAK142; Sigma, USA) and mitochondrial ROS levels in CMECs were measured using a Mitosox Red Mitochondrial Superoxide Indicator (M36008; Invitrogen, USA) according to the manufacturer's instructions. The fluorescent signal intensity was measured with a Nikon Eclipse Ti inverted fluorescence microscope (Nikon, Japan).

2.12. Western immunoblot

To obtain total protein extracts, cultured cells or frozen cardiac tissues were lysed at 4 °C in radioimmunoprecipitation (RIPA) buffer with cocktail protease inhibitor (Beyotime Biotechnology, China). Tissue homogenates or cell lysates were clarified by centrifugation at 12,000 rpm for 15 min at 4 °C and the supernatant protein concentration was determined using the bicinchoninic acid method (Beyotime Biotechnology, China). Proteins (20 μ g) were size-fractionated by sodium dodecyl sulphate polyacrylamide gel electrophoresis and transferred onto Immobilon polyvinylidene difluoride membranes. The membranes were blocked for 2 h with 5% Difco™ Skim Milk (BD Biosciences, USA) and then probed overnight at 4 °C with primary antibodies (Tbl.S3), followed by the secondary antibody for an hour with a 1:30,000 dilution of Dylight™ 800 4XPEG-conjugated goat anti-rabbit IgG (H + L) or goat anti-mouse IgG (H + L) (Cell Signaling Technology, USA). The results were visualized and analyzed by Odyssey Infrared Imaging System (LICOR, USA).

2.13. Transcription activity of NF- κ B p65

Nuclear extracts from CMECs were obtained using a nuclear extraction kit (Beyotime Biotechnology, China). The DNA binding activity of NF- κ B p65 in nuclear extracts was determined by using TransAM™ NF- κ B p65 Colorimetric kits (40,069; Active Motif, USA) in duplicate according to the manufacturer's protocol. The absorbance was read by a microplate reader (Bio-Tek, USA) at 450 nm.

2.14. Immunofluorescent staining

For the immunofluorescent staining of heart sections, the sections were deparaffinized and rehydrated by gradient elution using xylene and ethanol, followed by washing with PBS. Antigen retrieval was performed in Tris-EDTA solution for 20 min at 95 °C. For the immunofluorescent staining of CMECs, cells were rinsed with PBS, fixed with 4% paraformaldehyde for 20 min at room temperature. Prepared heart sections or cells were blocked by incubation with 5% goat serum (Beyotime Biotechnology, China) for 1 h at 37 °C and incubated with primary antibodies (Tbl. S3) overnight at 4 °C. Slides were washed three times and incubated with Alexa Fluoro®594 conjugated anti-rabbit IgG and Alexa Fluoro®488 conjugated anti-mouse IgG (Cell Signaling Technology, USA) for 1 h at room temperature, at a 1:1000 dilution. Nuclei were stained using 4,6-diamidino-2-phenylindole (DAPI) for 5 min at room temperature. Stained heart sections or cells were observed using Nikon Eclipse Ti inverted confocal microscope (Nikon, Japan) and

analyzed using Image J software.

2.15. Transmission electron microscopy (TEM)

For TEM morphological analysis, freshly excised heart tissues or cell pellets were fixed in 2.5% glutaraldehyde in 0.1 M sodium cacodylate buffer (pH 7.4) at 4 °C for 2 h. After being washed with 0.1 M sodium cacodylate buffer, they were post-fixed with 1% osmium tetroxide for 2 h and dehydrated through a graded ethanol series at 4 °C. Finally, the samples were embedded in epoxy resin at room temperature for 4 h. Ultrathin sections (70 nm) were assembled to a copper grid and observed using electron microscopy (Hitachi, Japan).

2.16. Statistical analysis

Statistical analysis was performed by using SPSS 22.0 software. All arithmetic data were presented as mean ± SD at least three independent experiments. The two-tailed t-test was used to analyze the differences

between 2 groups, and one-way ANOVA followed by Bonferroni post hoc test was used to analyze the differences among 3 or more groups. All P-value < 0.05 was considered statistically significant.

3. Results

3.1. Irisin ameliorated DOX-induced cardiac perivascular fibrosis by inhibiting EndMT

To explore whether irisin was a key mediator of the beneficial effects of exercise on DIC, we used a mouse model of chronic doxorubicin myocardial injury. The experimental design paradigm was shown in Fig. S1A. Echocardiography suggested that both ejection fraction (EF) and fraction shortening (FS) were significantly reduced after injection of DOX. Compared with the DOX group, EXE or injection of irisin can significantly ameliorate the reduction of cardiac function caused by DOX (Fig. 1A–C). HE staining demonstrated that cardiac tissue was badly damaged in the DOX group, as indicated by ruptured cardiomyocytes

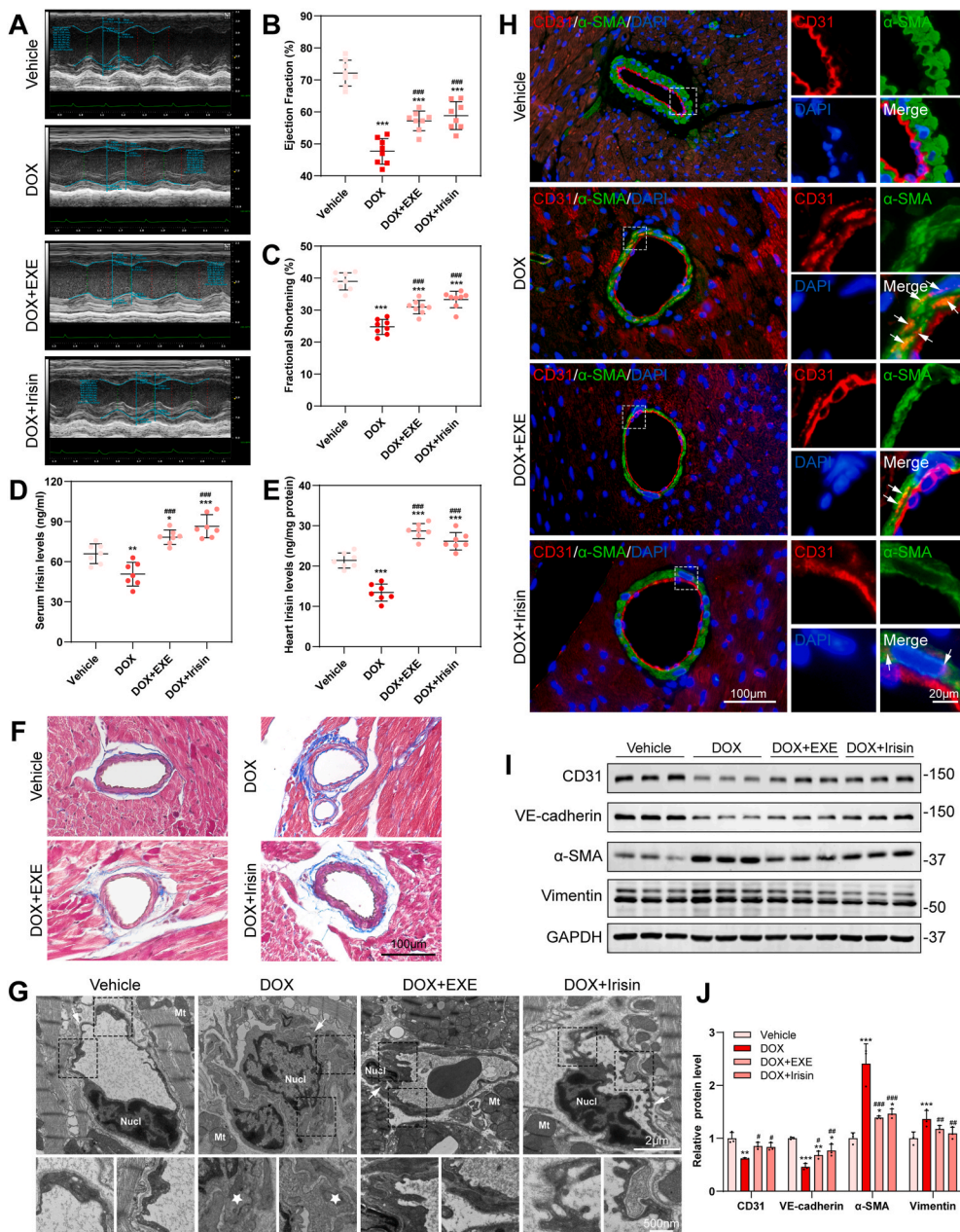


Fig. 1. Irisin ameliorated DOX-induced cardiac perivascular fibrosis by inhibiting EndMT. **A** Representative M-mode images of trans-thoracic echocardiography. **B, C** Quantification of ejection fraction (EF) and fraction shortening (FS) (n = 8). **D, E** Serum irisin level and heart irisin level were detected by ELISA (n = 7). **F** Representative images of MASSON staining of perivascular fibrosis in heart sections. **G** The ultrastructure of the heart capillaries was assessed using transmission electron microscopy. White arrows indicate the basement membrane. White pentangles indicate the migration in the intima. **H** Representative images of immunofluorescence double-staining of α -SMA (green) and CD31 (red) in heart sections. The cell nuclei were stained with DAPI (blue). White arrows indicate CD31 appearing in the smooth muscle layer. **I, J** Representative blots and quantitative analysis of endothelial-to-mesenchymal transition (EndMT) markers in mice myocardium (n = 3). The data are expressed as mean \pm SD, *p < 0.05, **p < 0.01 and ***p < 0.001 vs. Vehicle group; #p < 0.05, ##p < 0.01 and ###p < 0.001 vs. DOX group (one-way ANOVA followed by Bonferroni post hoc test). (For interpretation of the references to colour in this figure legend, the reader is referred to the Web version of this article.)

and disordered myocardial fibers. Notably, both EXE and irisin injection alleviated the abnormal morphological alterations of cardiomyocytes (Fig. S1B). Besides, both serum irisin and myocardial tissue irisin levels of mice in the DOX group were significantly reduced, which were reversed by EXE or irisin injection (Fig. 1D and E). Previous studies have shown the protective effect of FNDC5/irisin on cardiomyocytes. But interestingly, in Masson trichrome staining, we found that in the early stage of DIC (2 weeks after last DOX injection), fibrosis appeared around the heart capillaries, while fibrosis between cardiomyocytes was not obvious until a late stage (4 weeks after last DOX injection), and the DOX-induced cardiac perivascular fibrosis can be partially reversed by EXE or irisin injection (Fig. 1F and Fig. S1C).

Previous studies have shown that microvascular endothelial cell

dysfunction plays an important role in perivascular fibrosis. To study the role of CMECs in DOX-induced perivascular fibrosis, we observed the ultrastructure of CMECs through an electron microscope. As presented in Fig. 1G, CMECs were flat, elongated, and separated from smooth muscle cells via a thick basement membrane in the vehicle group and EXE or irisin injection group. In the DOX group, CMECs lost the complete basement membrane, displayed migration in the intima, and alter their nuclei orientation, which showed an ultrastructural characteristic of EndMT. To further determine, double immunofluorescent staining was used for CD31 and α -SMA in the heart tissue sections (Fig. 1H). Red-stained CD31 positive ECs laid on the inner wall of the lumen continuously and completely in the vehicle group. However, in the DOX group, it became intermittent and appeared in the smooth muscle layer marked

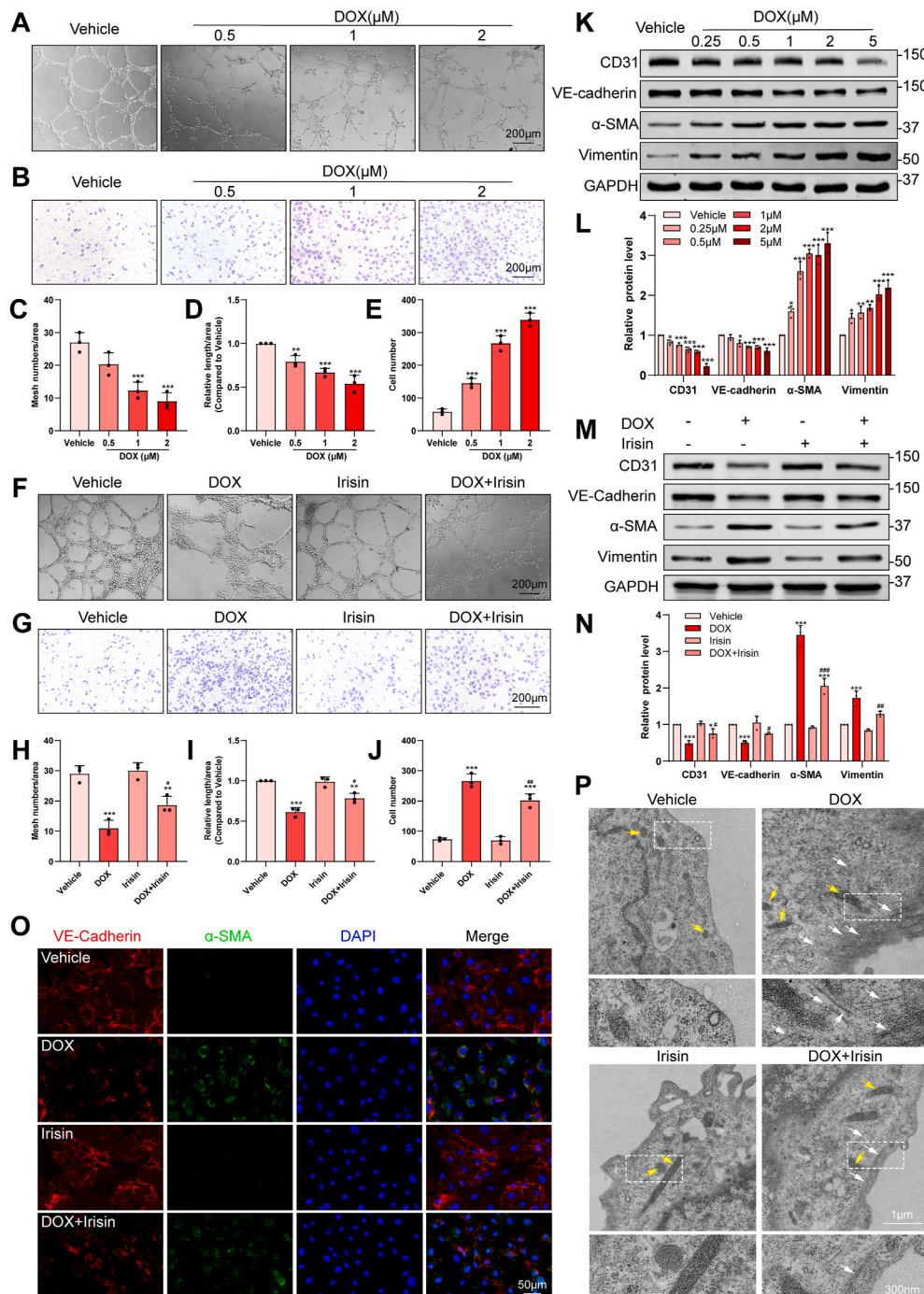


Fig. 2. Irisin ameliorated DOX-induced endothelial dysfunction of CMECs by inhibiting EndMT.

A Representative images of the ring structures of CMECs treated with different concentrations of DOX for 48 h. The mesh number (C) and tube length (D) were analyzed using ImageJ software. **B** Representative images of a transwell assay of the CMECs migration response to different concentrations of DOX for 48 h. The number of migrated cells (E) was quantified using ImageJ software. **F** Representative images of the vascular structures of CMECs treated with DOX (1 μ M) and/or irisin (20 nM) for 48 h. The mesh number (H) and tube length (I) were analyzed using ImageJ software. **G** Representative images of a transwell assay of the CMECs migration response to DOX (1 μ M) and/or irisin (20 nM) for 48 h. The number of migrated cells (J) was quantified using ImageJ software. **K, L** Representative blots and quantitative analysis of western blotting analysis of EndMT markers in CMECs treated with different concentrations of DOX for 48 h. **M, N** Representative blots and quantitative analysis of western blotting analysis of EndMT markers in CMECs treated with DOX (1 μ M) and/or irisin (20 nM) for 48 h. **O** Representative images of immunofluorescence double-staining of α -SMA (green) and VE-cadherin (red) in CMECs treated with DOX (1 μ M) and/or irisin (20 nM) for 48 h. The cell nuclei were stained with DAPI (blue). **P** The ultrastructure of the CMECs treated with DOX (1 μ M) and/or irisin (20 nM) for 48 h was assessed using transmission electron microscopy. Yellow arrows indicate the Weibel-Palade bodies. White arrows indicate microfilaments in the cytoplasm. The data are presented as the Mean \pm SD of three independent experiments. * p < 0.05, ** p < 0.01 and *** p < 0.001 vs. Vehicle group; # p < 0.05, ## p < 0.01 and ### p < 0.001 vs. DOX group (one-way ANOVA followed by Bonferroni post hoc test). (For interpretation of the references to colour in this figure legend, the reader is referred to the Web version of this article.)

in green-stained α -SMA. This phenomenon was partially reversed by EXE or irisin injection. What's more, DOX significantly reduced the expression of the ECs makers (CD31 and VE-cadherin) and upregulated the expression of mesenchymal cell markers (α -SMA and Vimentin) in the heart, which were partially reversed by EXE or irisin injection (Fig. 1I and J). Together, these results suggested that DOX caused cardiac perivascular fibrosis by the EndMT process in the early stage of DIC, and irisin might be a key mediator of the beneficial effects of EXE to restrain the process of EndMT induced by DOX.

3.2. Irisin ameliorated DOX-induced endothelial dysfunction of CMECs by inhibiting EndMT

To further verify the role of EndMT in DOX-induced endothelial dysfunction and whether irisin can reverse this phenomenon, mouse CMECs were extracted, identified by immunofluorescence of CD31

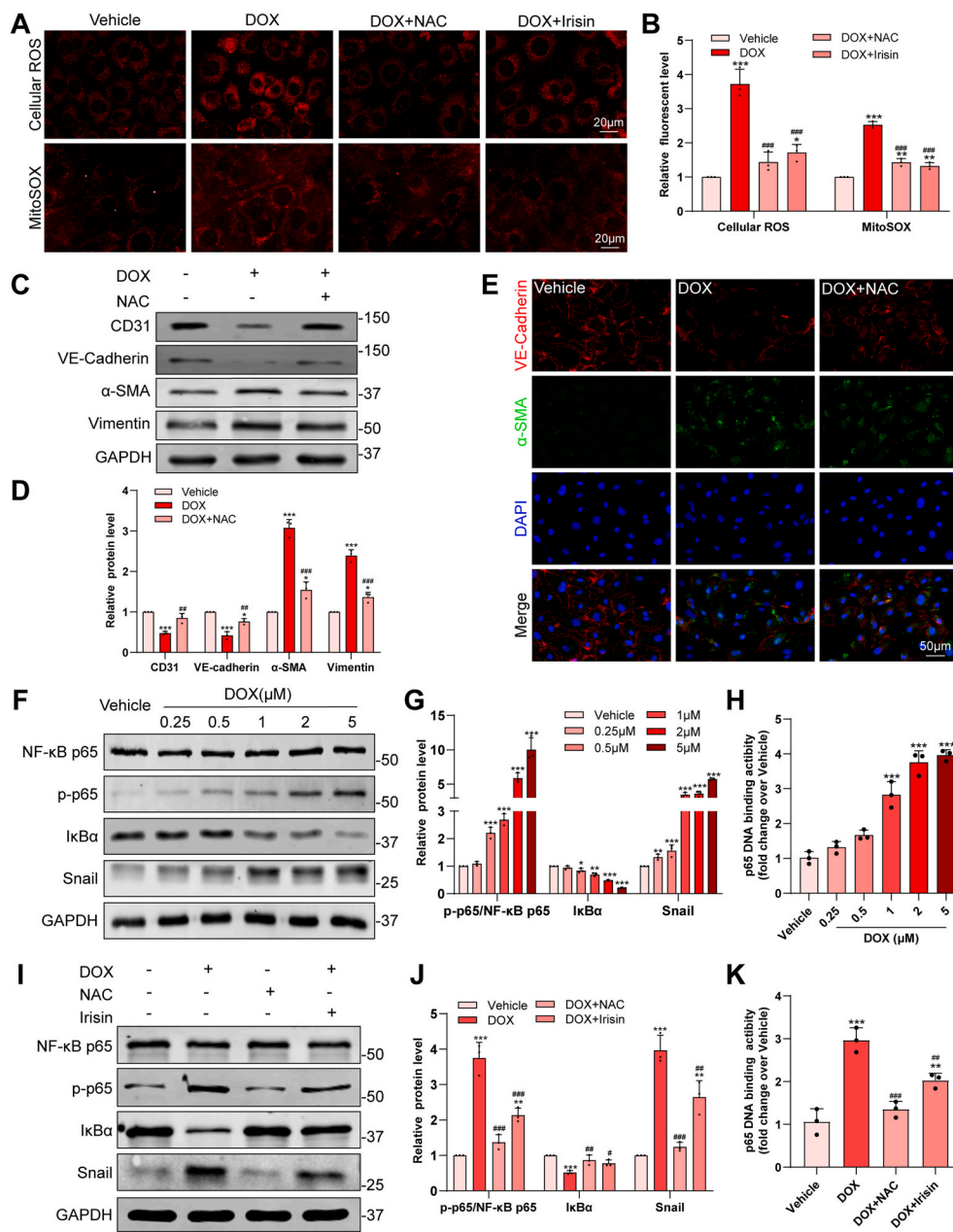


Fig. 3. Irisin attenuated DOX-induced EndMT by inhibiting ROS-induced NF- κ B-Snail activation.

A, B Representative images and quantification of cellular ROS and MitoSOX levels in CMECs treated with different concentrations of DOX for 48 h. **C, D** Representative blots and quantitative analysis of western blotting analysis of EndMT markers in CMECs pretreated with NAC before DOX treatment. **E** Representative images of immunofluorescence double-staining of α -SMA (green) and VE-cadherin (red) in CMECs pretreated with NAC before DOX treatment. The cell nuclei were stained with DAPI (blue). **F, G** Representative blots and quantitative analysis of western blotting analysis of NF- κ B-Snail signaling pathway in CMECs treated with different concentrations of DOX for 48 h. **H** p65 DNA binding activity was measured in CMECs treated with different concentrations of DOX for 48 h. **I, J** Representative blots and quantitative analysis of western blotting analysis of NF- κ B-Snail signaling pathway in CMECs pretreated with NAC or irisin before DOX treatment. **K** p65 DNA binding activity was measured in CMECs pretreated with NAC or irisin before DOX treatment. The data are presented as the Mean \pm SD of three independent experiments. * $p < 0.05$, ** $p < 0.01$ and *** $p < 0.001$ vs. Vehicle group; # $p < 0.05$, ## $p < 0.01$ and ### $p < 0.001$ vs. DOX group (one-way ANOVA followed by Bonferroni post hoc test). (For interpretation of the references to colour in this figure legend, the reader is referred to the Web version of this article.)

mesenchymal cells, as characterized by both the mixed features of ECs (Weibel-Palade bodies) and the characteristic of mesenchymal cells (microfilaments). Irisin treatment partially reversed the ultrastructural shift and maintained the endothelial character. These results suggested that DOX caused CMECs dysfunction by promoting EndMT, which could be partially reversed by irisin pretreatment.

3.3. Irisin attenuated DOX-induced EndMT by inhibiting ROS-induced NF- κ B-Snail activation

The traditional mechanisms of EndMT mainly involved the upregulation of TGF- β /Smads, but it has not changed significantly in our results (Figs. S3A and B). Oxidative stress also contributed to vascular remodeling [10]. To confirm the role of ROS in DOX-induced EndMT, we pretreated CMECs with N-acetyl-L-cysteine (NAC, an anti-oxidant agent) before DOX treated. Our results showed an increased cellular ROS level in DOX-treated CMECs, which were significantly reversed by NAC (Fig. 3A and B). Since mitochondria were the main source of ROS. We detected mitoSOX in the DOX-treated CMECs and found the same trend (Fig. 3A and B). Besides, NAC exerted a remarkable reversal, by decreasing mesenchymal biomarkers and enhancing endothelial biomarkers (Fig. 3C–E). Irisin pretreated also showed a decreased level of cellular ROS and mitoSOX (Fig. 3A and B), suggesting that the anti-EndMT effect of irisin depended on ROS inhibition.

The activation of the NF- κ B-Snail signaling pathway has been reported to contribute to the development of EndMT [24], and NF- κ B is also a transcriptional factor regulated by excessive ROS [25]. Therefore, the role of irisin in regulating the NF- κ B-Snail pathway in DOX-induced EndMT was accessed. The results showed that DOX significantly promoted the activation of NF- κ B and the subsequent transcription of Snail in a dose-dependent manner, demonstrated by an increased level of phospho-p65, a decreased level of I κ B α (Fig. 3F and G), excessive DNA binding activity of p65 (Fig. 3H) and the consequent upregulation of Snail expression (Fig. 3F and G). The activation of the NF- κ B-Snail signaling pathway was significantly inhibited by pretreatment with irisin or NAC (Fig. 3I–K). Together, these results suggested that irisin attenuated DOX-induced EndMT by inhibiting ROS-induced NF- κ B-Snail activation.

3.4. Irisin inhibited ROS accumulation by promoting autophagy to ameliorate DOX-induced EndMT

Given that DOX caused dysregulation of autophagy in cardiomyocytes [13], and exercise resulted in upregulation of autophagy in many tissues [26]. To explore whether irisin played a role in regulating autophagy as exercise, autophagy-related proteins were detected in the heart tissue of the mouse model. Compared to the vehicle group, the DOX group showed a decreased expression of Beclin-1 and LC3B-II, with the upregulation of p62, which were significantly reversed both by EXE and irisin injection (Fig. 4A and B). Then, we performed autophagy detection on CMECs stimulated by different concentrations of DOX. Western blot showed that DOX significantly reduced the expression of LC3B-II and Beclin-1 and upregulated the expression of p62 in a dose-dependent manner (Fig. 4C and D). The GFP-LC3B transfected CMECs also showed an inhibition of autophagy flux by DOX (Fig. 4E and H). Compared to the DOX group, CMECs pretreated with RAPA (an autophagy activator, Figs. S4A and B) showed a decreased cellular ROS and mitoSOX level, and CMECs pretreated 3-MA (an autophagy inhibitor, Figs. S4A and B) showed an increased ROS level (Fig. F and G) based on DOX treatment. The activation of the NF- κ B-Snail signaling pathway also changed accordingly (Fig. 4I–K). Further, the phenotype of EndMT

was also tested and the results revealed that up-regulation of autophagy partially restored endothelial biomarkers and decreased mesenchymal biomarkers in CMECs treated with DOX. And autophagy inhibition had a more serious EndMT phenotype (Fig. 4L–N). Interestingly, Irisin pretreated partially rescued the autophagy disorder in CMECs (Fig. 4O–R). Altogether, these results revealed that autophagy could inhibit DOX-induced EndMT by ROS clearance, and irisin can partially reverse the autophagy disorder induced by DOX.

3.5. UCP2 was involved in the regulation of EndMT of irisin

Irisin was firstly found to modulate UCP1 expression and act on the mitochondrial biogenesis in white adipose tissue [19]. As compared with the other members of the UCP family, UCP2 shares 55–60% homology with UCP1 and is widely expressed in various organizations [27]. We found that DOX-treatment reduced the expression of UCP2 both in mouse heart tissue (Fig. 5A and C) and CMECs (Figs. S5A and B), and pretreated -irisin partially restored UCP2 expression (Fig. 5A–D). For further verification, the siRNA for UCP2 was constructed and transfected into CMECs. The transfection efficiency was shown in Figs. S5C–E. Under the stimulation of DOX, compared to siNC group, the siUCP2 transfection showed more cellular ROS and mitoSOX accumulation (Fig. 5E and F), higher NF- κ B-Snail signaling pathway activity (Fig. 5G–I), and the phenomenon of EndMT was more serious (Fig. 5J, K and O), which could not be reversed by irisin. Besides, the siUCP2 transfection also showed an inhibition of autophagy, demonstrated by an increased level of Beclin-1 and LC3B-II, a decreased level of p62 (Fig. 5L and M), and a reduction of autophagy flux (Fig. 5N and P), which could not be reversed by irisin. These results suggested that UCP2 could be a potential target in the protective effect of irisin in DOX-induced EndMT.

3.6. Irisin mainly came from cardiomyocytes in the heart microenvironment and played a protective role against DOX-induced EndMT

A recent study showed that endogenous FNDC5/irisin in cardiomyocytes had a potential protective effect on DOX-induced cardiomyocyte damage [20]. To verify whether irisin could act as a cardiac factor on endothelial cells in a paracrine manner in the cardiac microenvironment, we first detected that FNDC5 was specific expressed in cardiomyocytes in mouse heart tissue and was downregulated after DOX treated by double immunofluorescent staining of cTnT and FNDC5 (Fig. S6A). Later, mouse CMs and CFs were extracted, identified by immunofluorescence of cTnT (Fig. S6B) and Vimentin (Fig. S6C), and treated with DOX. Compared to CFs and CMECs, the expression of FNDC5 was more abundant in CMs, which was markedly reduced in response to DOX (Fig. 6A–C). We also examined irisin levels in culture supernatants and found that the supernatants of CMs contained more irisin than the supernatants of CFs and CMECs, which decreased with the intervention of doxorubicin (Fig. 6D). Hereafter, the siRNA for FNDC5 was constructed and transfected into CMs. The transfection efficiency was shown in Figs. S6D–F. Transfected CMs were co-cultured with CMECs and treated with DOX and exogenous irisin. Compared to the siNC group, the siFNDC5 transfected group showed a lower irisin level in co-cultured supernatant (Fig. S6G), accompanied by a decreased expression of UCP2 (Fig. 6G and H), more severe cellular ROS and mitoSOX accumulation (Fig. 6E and F), higher NF- κ B-Snail signaling pathway activity (Fig. 6G–I), the more obvious phenomenon of EndMT (Fig. 6J, K and N) and the lower level of autophagy (Fig. 6L, M, O, and P) in CMECs. All these changes could be partially reversed by exogenous irisin.

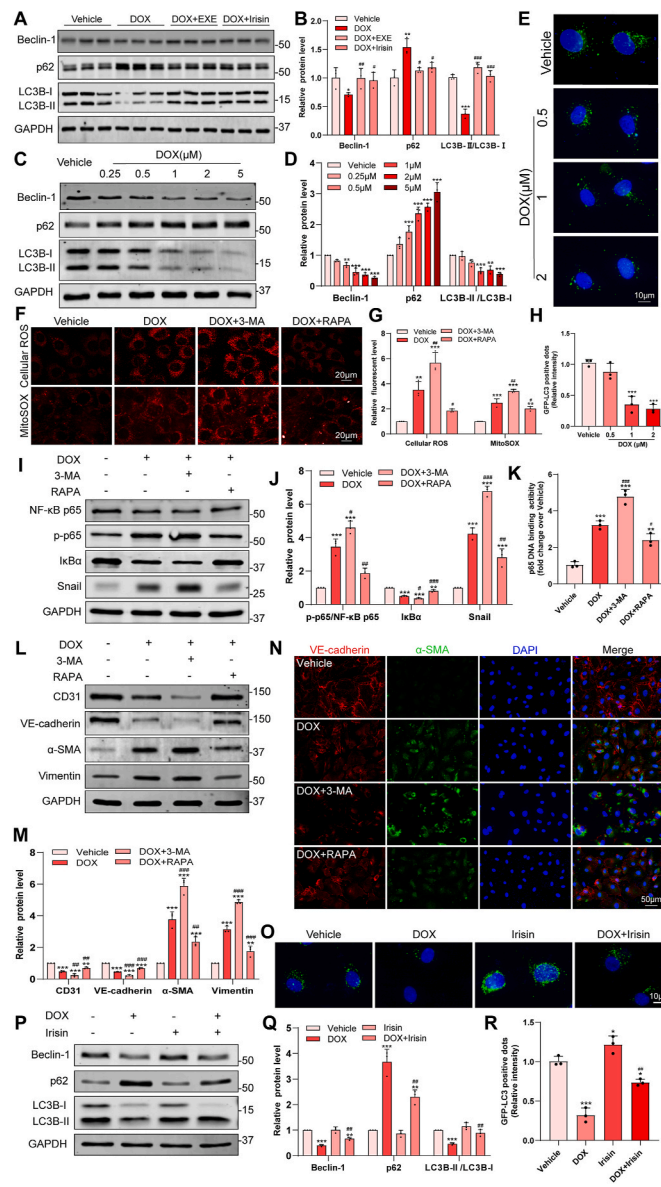


Fig. 4. Irisin inhibited ROS accumulation by promoting autophagy to ameliorate DOX-induced EndMT.

A, B Representative blots and quantitative analysis of western blotting analysis of autophagy-related proteins in mice myocardium. **C, D** Representative blots and quantitative analysis of western blotting analysis of autophagy-related proteins in CMECs treated with different concentrations of DOX for 48 h. **E** Representative fluorescence microscopy images of GFP-LC3 transfected CMECs treated with different concentrations of DOX for 48 h. The relative GFP-LC3 positive dots (**H**) were calculated according to the fluorescence intensity. **F, G** Representative images and quantification of cellular ROS and mitoSOX levels in CMECs pretreated with 3-MA or RAPA before DOX treatment. **I, J** Representative blots and quantitative analysis of western blotting analysis of NF-κB-Snail signaling pathway in CMECs pretreated with 3-MA or RAPA before DOX treatment. **K** p65 DNA binding activity was measured in CMECs pretreated with 3-MA or RAPA before DOX treatment. **L, M** Representative blots and quantitative analysis of western blotting analysis of EndMT markers in CMECs pretreated with 3-MA or RAPA before DOX treatment. **N** Representative images of immunofluorescence double-staining of α-SMA (green) and VE-cadherin (red) in CMECs pretreated with 3-MA or RAPA before DOX treatment. The cell nuclei were stained with DAPI (blue). **O** Representative fluorescence microscopy images of GFP-LC3 transfected CMECs treated with DOX (1 μM) and/or irisin (20 nM) for 48 h. The relative GFP-LC3 positive dots (**R**) were calculated according to the fluorescence intensity. **P, Q** Representative blots and quantitative analysis of western blotting analysis of autophagy-related proteins in CMECs treated with DOX (1 μM) and/or irisin (20 nM) for 48 h. The data are presented as the Mean ± SD of three independent experiments. *p < 0.05, **p < 0.01 and ***p < 0.001 vs. Vehicle group; #p < 0.05, ##p < 0.01 and ###p < 0.001 vs. DOX group (one-way ANOVA followed by Bonferroni post hoc test). (For interpretation of the references to colour in this figure legend, the reader is referred to the Web version of this article.)

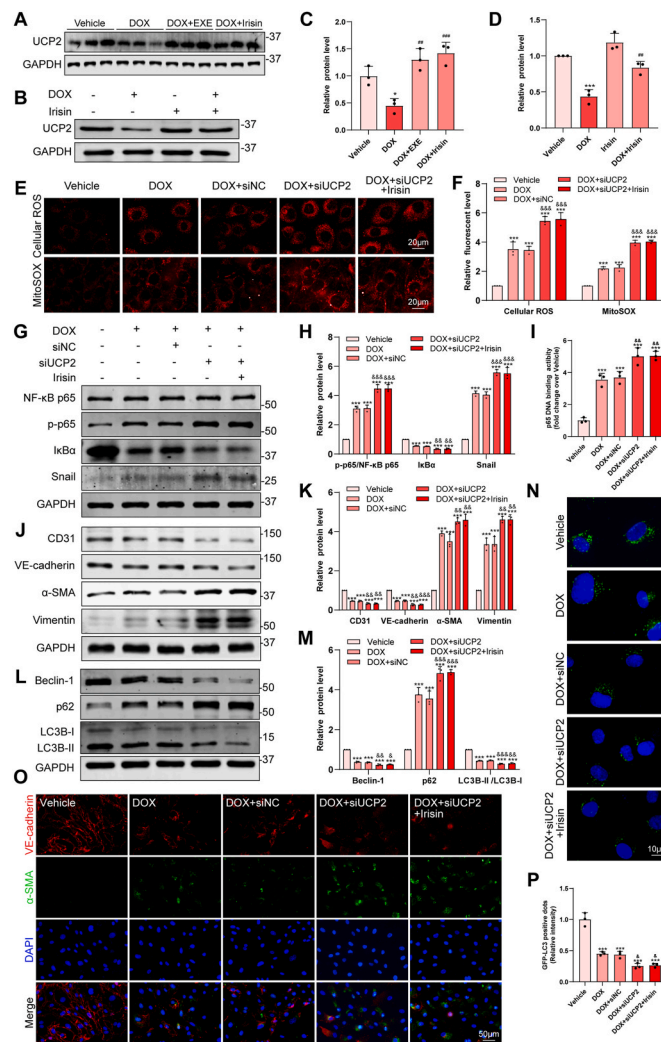


Fig. 5. UCP2 was involved in the regulation of EndMT of irisin. **A, C** Representative blots and quantitative analysis of western blotting analysis of UCP2 in mice myocardium. **B, D** Representative blots and quantitative analysis of western blotting analysis of UCP2 in CMECs treated with DOX (1 μ M) and/or irisin (20 nM) for 48 h. **E, F** Representative images and quantification of cellular ROS and mitoSOX levels in CMECs transfected with siUCP2 before DOX treatment. **G, H** Representative blots and quantitative analysis of western blotting analysis of NF- κ B-Snail signaling pathway in CMECs transfected with siUCP2 before DOX treatment. **I** p65 DNA binding activity was measured in CMECs transfected with siUCP2 before DOX treatment. **J, K** Representative blots and quantitative analysis of western blotting analysis of EndMT markers in CMECs transfected with siUCP2 before DOX treatment. **L, M** Representative blots and quantitative analysis of western blotting analysis of autophagy-related proteins in CMECs transfected with siUCP2 before DOX treatment. **O** Representative images of immunofluorescence double-staining of α -SMA (green) and VE-cadherin (red) in CMECs transfected with siUCP2 before DOX treatment. The cell nuclei were stained with DAPI (blue). **N** Representative fluorescence microscopy images of GFP-LC3 transfected CMECs transfected with siUCP2 before DOX treatment. The relative GFP-LC3 positive dots (**P**) were calculated according to the fluorescence intensity. The data are presented as the Mean \pm SD of three independent experiments. * p < 0.05, ** p < 0.01 and *** p < 0.001 vs. Vehicle group; # p < 0.05, ## p < 0.01 and ### p < 0.001 vs. DOX group; &# p < 0.05, &&# p < 0.01 and &&&# p < 0.001 vs. DOX + siNC group (one-way ANOVA followed by Bonferroni post hoc test). (For interpretation of the references to colour in this figure legend, the reader is referred to the Web version of this article.)

Finally, we specifically downregulated FNDC5 in the myocardium in vivo via a single injection of an AAV9 carrying FNDC5 shRNA. The transfection efficiency in the myocardium was shown in Figs. S7B–E. Compared to AAV9-NC, mice injected with AAV9-shFNDC5 showed more severe impairment of cardiac dysfunction under DOX treatment, which could be partially reversed by irisin injection (Fig. 7A–C). Both serum irisin and myocardial tissue irisin levels in the AAV9-shFNDC5 group were significantly reduced compared to AAV9-NC group, which were reversed by irisin injection (Fig. 7D and E). Additionally, FNDC5 deficiency increased the degree of perivascular fibrosis (Fig. 7F) and EndMT (Fig. 7G–I) as well as decreased the degree of autophagy (Fig. 7J and K). All these changes could be partially reversed by exogenous irisin. Collectively, we concluded that irisin from CMs attenuated DOX-induced EndMT in a paracrine manner.

4. Discussion

In the present study, we found that DOX-induced perivascular fibrosis in the early stage was associated with the program of EndMT. Irisin supplementation could alleviate perivascular fibrosis and EndMT in DIC. Mechanistically, we revealed that ROS-induced NF- κ B-Snail activation could be a potential way in DOX-induced EndMT, and autophagy disorder was responsible for the accumulation of ROS. Irisin treatment showed an anti-oxidant effect and ameliorated autophagy disorder by regulating UCP2, a proven target of irisin. Moreover, we initially explored the protective effect of irisin secreted by CMs on CMECs in the cardiac microenvironment, suggesting the possibility of irisin as a cardiokine. Collectively, we supposed that irisin was a

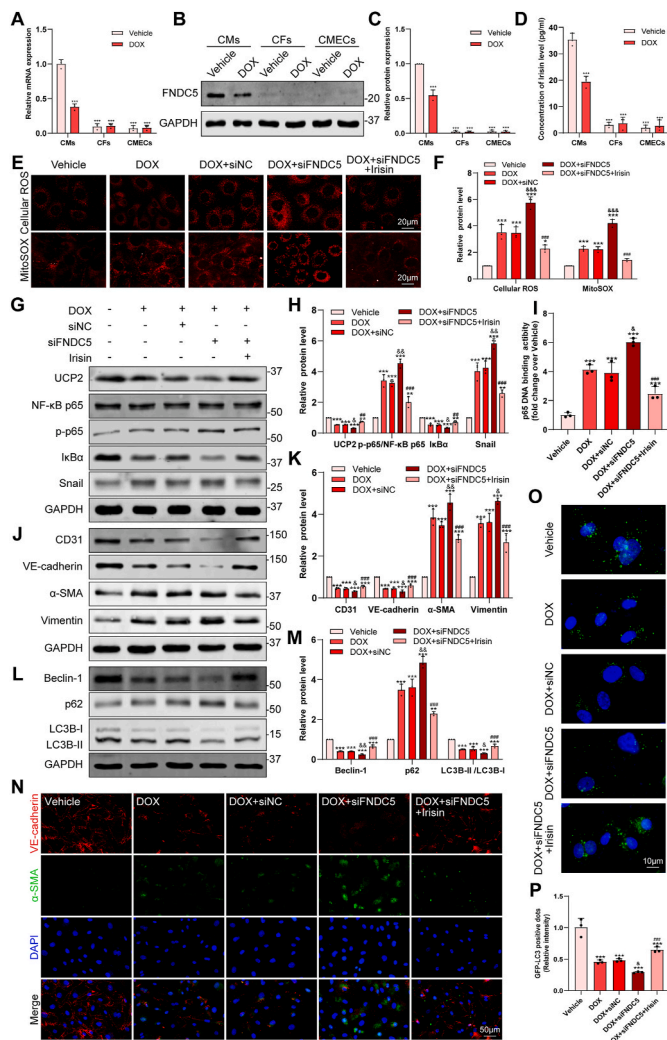


Fig. 6. Irisin mainly came from cardiomyocytes in the heart microenvironment and played a protective role against DOX-induced EndMT. **A-C** The expression of FNDC5 in isolated CMs, CFs, and CMECs. **D** The irisin levels in cultured supernatants from isolated CMs, CFs, and CMECs. Hereafter, CMs transfected with siFNDC5 were co-cultured with CMECs and treated with DOX and exogenous irisin. **E, F** Representative images and quantification of cellular ROS and mitoSOX levels in CMECs. **G, H** Representative blots and quantitative analysis of western blotting analysis of UCP2 and NF-κB-Snail signaling pathway in CMECs. **I** p65 DNA binding activity was measured in CMECs. **J, K** Representative blots and quantitative analysis of western blotting analysis of EndMT markers in CMECs. **L, M** Representative blots and quantitative analysis of western blotting analysis of autophagy-related proteins in CMECs. **N** Representative images of immunofluorescence double-staining of α-SMA (green) and VE-cadherin (red) in CMECs. The cell nuclei were stained with DAPI (blue). **O** Representative fluorescence microscopy images of GFP-LC3 transfected CMECs. The relative GFP-LC3 positive dots (**P**) were calculated according to the fluorescence intensity. The data are presented as the Mean ± SD of three independent experiments. **p* < 0.05, ***p* < 0.01 and ****p* < 0.001 vs. Vehicle group; &*p* < 0.05, &&*p* < 0.01 and &&&*p* < 0.001 vs. DOX + siNC group; #*p* < 0.05, ##*p* < 0.01 and ###*p* < 0.001 vs. DOX + siFNDC5 group (one-way ANOVA followed by Bonferroni post hoc test). (For interpretation of the references to colour in this figure legend, the reader is referred to the Web version of this article.)

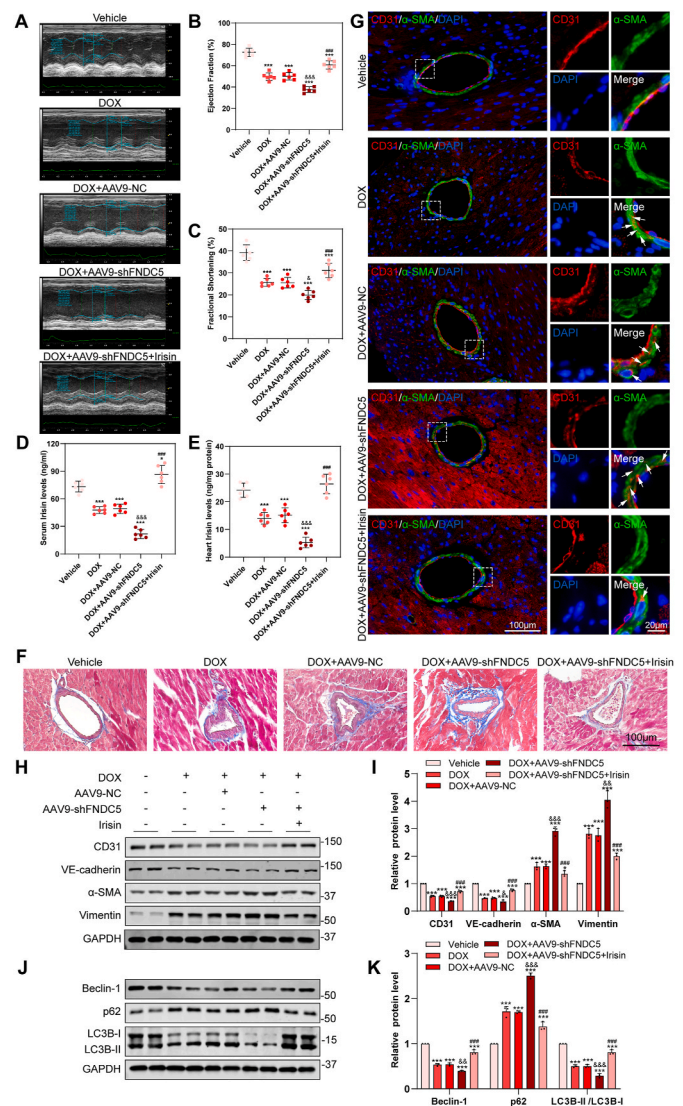


Fig. 7. Irisin mainly came from cardiomyocytes in the heart microenvironment and played a protective role against DOX-induced EndMT and cardiac perivascular fibrosis in vivo. **A** Representative M-mode images of transthoracic echocardiography. **B, C** Quantification of ejection fraction (EF) and fraction shortening (FS) (*n* = 6). **D, E** Serum irisin level and heart irisin level were detected by ELISA (*n* = 6). **F** Representative images of MASSON staining of perivascular fibrosis in heart sections. **G** Representative images of immunofluorescence double-staining of α-SMA (green) and CD31 (red) in heart sections. The cell nuclei were stained with DAPI (blue). White arrows indicate CD31 appearing in the smooth muscle layer. **H, I** Representative blots and quantitative analysis of western blotting analysis of EndMT markers in mice myocardium (*n* = 3). **J, K** Representative blots and quantitative analysis of western blotting analysis of autophagy-related proteins in mice myocardium (*n* = 3). The data are expressed as mean ± SD, **p* < 0.05, ***p* < 0.01 and ****p* < 0.001 vs. Vehicle group; &*p* < 0.05, &&*p* < 0.01 and &&&*p* < 0.001 vs. DOX + AAV9-NC group; #*p* < 0.05, ##*p* < 0.01 and ###*p* < 0.001 vs. DOX + AAV9-shFNDC5 group (one-way ANOVA followed by Bonferroni post hoc test). (For interpretation of the references to colour in this figure legend, the reader is referred to the Web version of this article.)

potential therapeutic agent against DOX-induced perivascular fibrosis.

As the cornerstone of chemotherapy regimens, anthracyclines are still greatly restricted due to their cardiotoxicity. Despite being widely studied, an important limitation of the current understanding of how DOX damages the heart is that almost all proposed mechanisms are concentrated in cardiomyocytes. Recent studies showed an increased LV myocardial extracellular volume (ECV) fraction, which represented cardiac fibrosis, in the early stage after the initiation of anthracycline chemotherapy in patients [28,29]. And in the mice DIC model, the sub-acute increase in fibrosis was strongly linked and was predictive of late mortality [30]. Previous explanations of the early fibrosis were the reactive fibrosis of CFs, but not replacement fibrosis [6]. However, in our chronic mice model, the early fibrosis appeared around the capillaries rather than the interstitium of myocardial cells, which suggested that vascular factors played a certain role in it. Studies have shown that DOX-induced ECs damage could trigger the development and progression of cardiomyopathy by decreasing the release and activity of key endothelial factors [31]. And biomarkers of endothelial injury predicted early asymptomatic DIC in breast cancer patients [32]. However, the relationship between endothelial dysfunction and perivascular fibrosis in DIC is rarely discussed. EndMT has been shown as a significant contributor to the fibrosis process of a variety of cardiovascular diseases [7]. Endothelial injury caused by hypertension or other factors led to the phenotypic changes of ECs and participated in the initiation of fibroblasts and the secretion of ECM protein in the occurrence and development of myocardial fibrosis [33]. Here, we found that EndMT is involved in the process of perivascular fibrosis in the early stage of DIC. The CMECs showed decreased endothelial markers and increased interstitial cell markers during DOX treatment, accompanied by the functional disorders of CMECs.

A recent study showed that the classic TGF- β /smads pathway was involved in DOX-induced EndMT of CMECs [34], which is inconsistent with our results. In their *in vitro* experiments, the phenotype of EndMT was not induced by DOX stimulation, but directly by TGF- β treatment, which was not rigorous. And the *in vivo* results might be affected by other cells in myocardial tissue. Numerous studies implied a central role for increased ROS production in the mechanism of doxorubicin-mediated ECs injury [35]. In addition to the traditional TGF- β -Smads pathway, oxidative stress is another factor that promoted EndMT. Specifically, hydrogen peroxide activated EndMT in HUVECs in an incremental and dose-responsive manner that was significantly more effective than TGF- β alone [36]. And the inhibition of ROS could decrease oxidative stress-induced EndMT *in vitro* [37]. Our results also showed an increased ROS level in endothelial cells treated with DOX. Interestingly, the elimination of ROS, whether by up-regulating autophagy or using antioxidants, significantly inhibited the EndMT process induced by DOX. NF- κ B has been shown to play an important role in cytokine-induced EndMT [38], but it should be emphasized that the activation of NF- κ B can be induced not only by cytokines. Our previous studies have shown that H₂S induced NF- κ B inactivation and consequently caused the transcriptional inhibition of Snail, resulting in the reversal of EndMT in monocrotaline-induced pulmonary arterial hypertension [24]. The ROS-driven NF- κ B activation was also explored in angiotensin II-induced EndMT [10]. Consistent with this, we found that DOX stimulated the accumulation of ROS, activated the NF- κ B-Snail pathway, and triggered EndMT in CMECs.

The positive clinical effects of an exercise intervention on cardiac function have been well addressed [39]. In DIC, a large number of animal experiments have shown that exercise can effectively ameliorate cardiac dysfunction caused by DOX [40], with the mechanism involving improving mitochondrial function [41,42], regulating autophagy disorders [41,43], reducing oxidative stress levels [42,43], and improving

myocardial fibrosis [44]. This opened up a new situation for the prevention and treatment of DIC. However, it was hard to transform to the clinic with the bottleneck that the patients undergoing chemotherapy were too weak to tolerate effective exercise intensity. Therefore, new ingredients need to be found to partially replace the benefits of exercise. Irisin is a new hormone-like factor mainly released by muscles in response to exercise [19]. An increasing number of studies have shown the association of irisin and cardiovascular diseases [45,46]. Recently, the cardio-protected effect in DIC has been preliminarily confirmed, with the mechanism of reducing oxidative stress in cardiomyocytes by regulating the Akt pathway [20]. In addition, the inhibitory effect of irisin on EndMT of CMECs has also been reported in diabetic cardiomyopathy [22]. And irisin could suppress the migration, proliferation, and invasion of tumor cells by inhibiting EMT progress [47,48]. In this study, we found that irisin alleviated excessive ROS generation, suppressed NF- κ B activation, and attenuated EndMT of CMECs in DIC, thereby reduced the early perivascular fibrosis. Further, researchers observed that the expression of FNDC5 was abundant in the myocardium as skeletal muscle, suggesting irisin might be a cardiokine and exert the cardioprotective effect in autocrine or paracrine manners [20]. Here, we preliminarily studied the main cell types that secrete irisin in the heart and found that irisin from CMs had a paracrine protective effect on ECs.

The protective effect of irisin on DOX-induced EndMT of CMECs involved UCP2-related ROS regulation. UCP family-mediated antioxidant protection and its impairment are expected to play a major role in cell physiology and pathology [49]. Irisin was originally found to participate in the browning of WAT by up-regulating UCP1 in adipocytes [19]. UCP2 shares 55–60% similarity with UCP1, and were richly expressed in endothelial cells [50]. UCP2 has been suggested to participate in attenuation of the ROS production in heart [51–53] and to inhibit ROS-mediated apoptosis of CMs in DIC [52]. What's more, irisin showed a protective effect in pulmonary ischemia/reperfusion injury by targeting UCP2 [54]. Our present study found that the ROS elimination and the EndMT reversal by irisin depended on UCP2. This protective effect was greatly reduced in UCP2 knockdown CMECs, suggesting that UCP2 was involved in the regulation of EndMT of irisin.

In summary, our study provided strong support that ROS accumulation and autophagy disorders caused an EndMT in CMECs, which played a role in the perivascular fibrosis of DIC. Irisin treatment could partially reverse this phenomenon by regulating UCP2. As an exercise hormone, irisin was a key mediator of the beneficial effects of exercise and provided a new idea for the prevention of DIC. However, there were still some limitations to the current research. Firstly, a tissue-specific knockout mice model was lacking, although we used AAV to perform the knockdown verification to strengthen the data. Secondly, despite various methods that have been used to prove EndMT, it is still necessary to construct a lineage tracing system in mice in future research. Finally, we initially discussed the possibility of irisin as a cardiokine, and its regulation methods and effects in the entire cardiac microenvironment still need to further explore.

Funding

This work was supported by the National Natural Science Foundation of China (Grant No. 82070381 to Jun Gu and Grant No. 81870264 to Chang-qian Wang) and research projects from the Shanghai Science and Technology Commission (Grant No. 20ZR1431100 to Jun Gu).

Declaration of competing interest

The authors declare that they have no conflict of interest.

Appendix A. Supplementary data

Supplementary data to this article can be found online at <https://doi.org/10.1016/j.redox.2021.102120>.

References

- [1] S. Rivankar, An overview of doxorubicin formulations in cancer therapy, *J. Canc. Res. Therapeut.* 10 (2014) 853–858.
- [2] J.L. Zamorano, P. Lancellotti, D. Rodriguez Muñoz, V. Aboyans, R. Asteggiano, M. Galderisi, G. Habib, D.J. Lenihan, G.Y.H. Lip, A.R. Lyon, T. Lopez Fernandez, D. Mohty, M.F. Piepoli, J. Tamargo, A. Torbicki, T.M. Suter, ESC Scientific Document Group, 2016 ESC Position Paper on cancer treatments and cardiovascular toxicity developed under the auspices of the ESC Committee for Practice Guidelines: The Task Force for cancer treatments and cardiovascular toxicity of the European Society of Cardiology (ESC), *Eur. Heart J.* 37 (2016) 2768–2801.
- [3] P. Vejpongsa, E.T.H. Yeh, Prevention of anthracycline-induced cardiotoxicity: challenges and opportunities, *J. Am. Coll. Cardiol.* 64 (2014) 938–945.
- [4] D. Cappetta, F. Rossi, E. Piegari, F. Quaini, L. Berrino, K. Urbanek, A. De Angelis, Doxorubicin targets multiple players: a new view of an old problem, *Pharmacol. Res.* 127 (2018) 4–14.
- [5] B.N. Bernaba, J.B. Chan, C.K. Lai, M.C. Fishbein, Pathology of late-onset anthracycline cardiomyopathy, *Cardiovasc. Pathol.* 19 (2010) 308–311.
- [6] R. Tanaka, M. Umemura, M. Narikawa, M. Hikichi, K. Osawa, T. Fujita, U. Yokoyama, T. Ishigami, K. Tamura, Y. Ishikawa, Reactive fibrosis precedes doxorubicin-induced heart failure through sterile inflammation, *ESC Heart Fail* 7 (2020) 588–603.
- [7] E.M. Zeisberg, O. Tarnavski, M. Zeisberg, A.L. Dorfman, J.R. McMullen, E. Gustafsson, A. Chandraker, X. Yuan, W.T. Pu, A.B. Roberts, E.G. Neilson, M. H. Sayegh, S. Izumo, R. Kalluri, Endothelial-to-mesenchymal transition contributes to cardiac fibrosis, *Nat. Med.* 13 (2007) 952–961.
- [8] G. Sánchez-Duffhues, A. García de Vinuesa, P. ten Dijke, Endothelial-to-mesenchymal transition in cardiovascular diseases: developmental signaling pathways gone awry: endothelial Plasticity in Human Vascular Disorders, *Dev. Dynam.* 247 (2018) 492–508.
- [9] T. Wen, L. Du, B. Chen, D. Yan, A. Yang, J. Liu, N. Gu, J. Meng, H. Xu, Iron oxide nanoparticles induce reversible endothelial-to-mesenchymal transition in vascular endothelial cells at acutely non-cytotoxic concentrations, *Part. Fibre Toxicol.* 16 (2019) 30.
- [10] S. You, J. Qian, G. Wu, Y. Qian, Z. Wang, T. Chen, J. Wang, W. Huang, G. Liang, Schizandrin B attenuates angiotensin II induced endothelial to mesenchymal transition in vascular endothelium by suppressing NF- κ B activation, *Phytomedicine Int J Phytother Phytopharm* 62 (2019) 152955.
- [11] A.Z. Luu, B. Chowdhury, M. Al-Omran, H. Teoh, D.A. Hess, S. Verma, Role of endothelium in doxorubicin-induced cardiomyopathy, *JACC Basic Transl Sci* 3 (2018) 861–870.
- [12] J. Gu, Y.-Q. Fan, H.-L. Zhang, J.-A. Pan, J.-Y. Yu, J.-F. Zhang, C.-Q. Wang, Resveratrol suppresses doxorubicin-induced cardiotoxicity by disrupting E2F1 mediated autophagy inhibition and apoptosis promotion, *Biochem. Pharmacol.* 150 (2018) 202–213.
- [13] J.-A. Pan, Y. Tang, J.-Y. Yu, H. Zhang, J.-F. Zhang, C.-Q. Wang, J. Gu, miR-146a attenuates apoptosis and modulates autophagy by targeting TAF9b/P53 pathway in doxorubicin-induced cardiotoxicity, *Cell Death Dis.* 10 (2019) 668.
- [14] H.-T. Chen, H. Liu, M.-J. Mao, Y. Tan, X.-Q. Mo, X.-J. Meng, M.-T. Cao, C.-Y. Zhong, Y. Liu, H. Shan, G.-M. Jiang, Crosstalk between autophagy and epithelial-mesenchymal transition and its application in cancer therapy, *Mol. Canc.* 18 (2019) 101.
- [15] M. Huang, W. Xin, Matrine inhibiting pancreatic cells epithelial-mesenchymal transition and invasion through ROS/NF- κ B/MMPs pathway, *Life Sci.* 192 (2018) 55–61.
- [16] Y. Takagaki, S.M. Lee, Z. Dongqing, M. Kitada, K. Kanasaki, D. Koya, Endothelial autophagy deficiency induces IL6 - dependent endothelial mesenchymal transition and organ fibrosis, *Autophagy* 16 (2020) 1905–1914.
- [17] J. Zou, Y. Liu, B. Li, Z. Zheng, X. Ke, Y. Hao, X. Li, X. Li, F. Liu, Z. Zhang, Autophagy attenuates endothelial-to-mesenchymal transition by promoting Snail degradation in human cardiac microvascular endothelial cells, *Biosci. Rep.* 37 (2017).
- [18] J.M. Scott, A. Khakoo, J.R. Mackey, M.J. Haykowsky, P.S. Douglas, L.W. Jones, Modulation of anthracycline-induced cardiotoxicity by aerobic exercise in breast cancer: current evidence and underlying mechanisms, *Circulation* 124 (2011) 642.
- [19] P. Boström, J. Wu, M.P. Jedrychowski, A. Korde, L. Ye, J.C. Lo, K.A. Rasbach, E. A. Boström, J.H. Choi, J.Z. Long, S. Kajimura, M.C. Zingaretti, B.F. Vind, H. Tu, S. Cinti, K. Højlund, S.P. Gygi, B.M. Spiegelman, A PGC1- α -dependent myokine that drives brown-fat-like development of white fat and thermogenesis, *Nature* 481 (2012) 463–468.
- [20] X. Zhang, C. Hu, C.-Y. Kong, P. Song, H.-M. Wu, S.-C. Xu, Y.-P. Yuan, W. Deng, Z.-G. Ma, Q.-Z. Tang, FNDC5 alleviates oxidative stress and cardiomyocyte apoptosis in doxorubicin-induced cardiotoxicity via activating AKT, *Cell Death Differ.* 27 (2020) 540–555.
- [21] M. Pesce, P. Ballerini, T. Paolucci, I. Puca, M.H. Farzaei, A. Patrino, Irisin and autophagy: first update, *Int. J. Mol. Sci.* 21 (2020) E7587.
- [22] X. Liu, H. Mujahid, B. Rong, Q. Lu, W. Zhang, P. Li, N. Li, E. Liang, Q. Wang, D. Tang, N. Li, X. Ji, Y. Chen, Y. Zhao, M. Zhang, Irisin inhibits high glucose-induced endothelial-to-mesenchymal transition and exerts a dose-dependent bidirectional effect on diabetic cardiomyopathy, *J. Cell Mol. Med.* 22 (2018) 808–822.
- [23] V. Schefer, M.I. Talan, Oxygen consumption in adult and AGED C57BL/6J mice during acute treadmill exercise of different intensity, *Exp. Gerontol.* 31 (1996) 387–392.
- [24] H. Zhang, L.-Z. Hao, J.-A. Pan, Q. Gao, J.-F. Zhang, R.K. Kankala, S.-B. Wang, A.-Z. Chen, H.-L. Zhang, Microfluidic fabrication of inhalable large porous microspheres loaded with H2S-releasing aspirin derivative for pulmonary arterial hypertension therapy, *J. Contr. Release* 329 (2021) 286–298.
- [25] K.B. Myant, P. Cammareri, E.J. McGhee, A.A. Ridgway, D.J. Huels, J.B. Cordero, S. Schwitala, G. Kalna, E.-L. Ogg, D. Athineos, P. Timpson, M. Vidal, G.I. Murray, F.R. Greten, K.I. Anderson, O.J. Sansom, ROS production and NF- κ B activation triggered by RAC1 facilitate WNT-driven intestinal stem cell proliferation and colorectal cancer initiation, *Cell Stem Cell* 12 (2013) 761–773.
- [26] K.A. Escobar, N.H. Cole, C.M. Mermier, T.A. VanDusseldorp, Autophagy and aging: maintaining the proteome through exercise and caloric restriction, *Aging Cell* 18 (2019), e12876.
- [27] A. Ledesma, M.G. de Lacoba, E. Rial, The mitochondrial uncoupling proteins, *Genome Biol.* 3 (2002). REVIEWS3015.
- [28] E.B. Tham, M.J. Haykowsky, K. Chow, M. Spavor, S. Kaneko, N.S. Khoo, J. J. Pagano, A.S. Mackie, R.B. Thompson, Diffuse myocardial fibrosis by T1-mapping in children with subclinical anthracycline cardiotoxicity: relationship to exercise capacity, cumulative dose and remodeling, *J. Cardiovasc. Magn. Reson.* 15 (2013) 48.
- [29] G.C. Meléndez, J.H. Jordan, R.B. D'Agostino, S. Vasu, C.A. Hamilton, W. G. Hundley, Progressive three-month increase in left ventricular myocardial extracellular volume fraction after receipt of anthracycline based chemotherapy, *JACC Cardiovasc Imaging* 10 (2017) 708–709.
- [30] H. Farhad, P.V. Staziaki, D. Addison, O.R. Coelho-Filho, R.V. Shah, R.N. Mitchell, B. Szilveszter, S.A. Abbasi, R.Y. Kwong, M. Scherrer-Crosbie, U. Hoffmann, M. Jerosch-Herold, T.G. Neilan, Characterization of the changes in cardiac structure and function in mice treated with anthracyclines using serial cardiac magnetic resonance imaging, *Circ Cardiovasc Imaging* 9 (2016).
- [31] M. Räsänen, J. Degerman, T.A. Nissinen, I. Miinalainen, R. Kerkelä, A. Siltanen, J. T. Backman, E. Mervaala, J.J. Hulmi, R. Kivela, K. Alitalo, VEGF-B gene therapy inhibits doxorubicin-induced cardiotoxicity by endothelial protection, *Proc. Natl. Acad. Sci. U. S. A.* 113 (2016) 13144–13149.
- [32] V.K. Todorova, P.-C. Hsu, J.Y. Wei, A. Lopez-Candales, J.Z. Chen, L.J. Su, I. Makhoul, Biomarkers of inflammation, hypercoagulability and endothelial injury predict early asymptomatic doxorubicin-induced cardiotoxicity in breast cancer patients, *Am J Cancer Res* 10 (2020) 2933–2945.
- [33] T. Wilhelm, X. Xu, X. Tan, M.S. Hulshoff, S. Maamari, S. Sossalla, M. Zeisberg, E. M. Zeisberg, Serelaxin alleviates cardiac fibrosis through inhibiting endothelial-to-mesenchymal transition via RXFP1, *Theranostics* 10 (2020) 3905–3924.
- [34] T.-H. Tsai, C.-J. Lin, C.-L. Hang, W.-Y. Chen, Calcitriol attenuates doxorubicin-induced cardiac dysfunction and inhibits endothelial-to-mesenchymal transition in mice, *Cells* 8 (2019) E865.
- [35] E.V. Grakova, S.N. Shilov, K.V. Kopeva, E.N. Berezikova, A.A. Popova, M. N. Neupokoeva, E.T. Ratushnyak, A.T. Teplyakov, Anthracycline-induced cardiotoxicity: the role of endothelial dysfunction, *Cardiology* 1–9 (2021).
- [36] S.M. Ervrard, L. Lecce, K.C. Michelis, A. Nomura-Kitabayashi, G. Pandey, K.-R. Purushothaman, V. d' Escamard, J.R. Li, L. Hadri, K. Fujitani, P.R. Moreno, L. Benard, P. Rimmele, A. Cohain, B. Mecham, G.J. Randolph, E.G. Nabel, R. Hajjar, V. Fuster, M. Boehm, J.C. Kovacic, Endothelial to mesenchymal transition is common in atherosclerotic lesions and is associated with plaque instability, *Nat. Commun.* 7 (2016).
- [37] J. Li, Q. Zhang, C. Ren, X. Wu, Y. Zhang, X. Bai, Y. Lin, M. Li, J. Fu, P. Kopylov, S. Wang, T. Yu, N. Wang, C. Xu, Y. Zhang, B. Yang, Low-intensity pulsed ultrasound prevents the oxidative stress induced endothelial-mesenchymal transition in human aortic endothelial cells, *Cell. Physiol. Biochem.* 45 (2018) 1350–1365.
- [38] L. Pérez, N. Muñoz-Durango, C.A. Riedel, C. Echeverría, A.M. Kaleris, C. Cabello-Verrugio, F. Simon, Endothelial-to-mesenchymal transition: cytokine-mediated pathways that determine endothelial fibrosis under inflammatory conditions, *Cytokine Growth Factor Rev.* 33 (2017) 41–54.
- [39] C.J. Lavie, R. Arena, D.L. Swift, N.M. Johannsen, X. Sui, D.-C. Lee, C.P. Earnest, T. S. Church, J.H. O'Keefe, R.V. Milani, S.N. Blair, Exercise and the cardiovascular system: clinical science and cardiovascular outcomes, *Circ. Res.* 117 (2015) 207–219.
- [40] M.I. Matos, E. da C. Rubini, F. de O. Meirelles, EB da Silva, Aerobic exercise and cardiac function of murines exposed to doxorubicin: a meta-analysis, *Arq. Bras. Cardiol.* 115 (2020) 885–893.
- [41] I. Marques-Aleixo, E. Santos-Alves, J.R. Torrella, P.J. Oliveira, J. Magalhães, A. Ascensão, Exercise and doxorubicin treatment modulate cardiac mitochondrial quality control signaling, *Cardiovasc. Toxicol.* 18 (2018) 43–55.
- [42] I. Marques-Aleixo, E. Santos-Alves, D. Mariani, D. Rizo-Roca, A.I. Padrão, S. Rocha-Rodrigues, G. Viscor, J.R. Torrella, R. Ferreira, P.J. Oliveira, J. Magalhães, A. Ascensão, Physical exercise prior and during treatment reduces sub-chronic doxorubicin-induced mitochondrial toxicity and oxidative stress, *Mitochondrion* 20 (2015) 22–33.

- [43] Y. Lee, I. Kwon, Y. Jang, L. Cosio-Lima, P. Barrington, Endurance exercise attenuates doxorubicin-induced cardiotoxicity, *Med. Sci. Sports Exerc.* 52 (2020) 25–36.
- [44] H.-L. Yang, P.-L. Hsieh, C.-H. Hung, H.-C. Cheng, W.-C. Chou, P.-M. Chu, Y.-C. Chang, K.-L. Tsai, Early moderate intensity aerobic exercise intervention prevents doxorubicin-caused cardiac dysfunction through inhibition of cardiac fibrosis and inflammation, *Cancers* 12 (2020).
- [45] Y.T. Zhao, J. Wang, N. Yano, L.X. Zhang, H. Wang, S. Zhang, G. Qin, P. M. Dubielecka, S. Zhuang, P.Y. Liu, Y.E. Chin, T.C. Zhao, Irisin promotes cardiac progenitor cell-induced myocardial repair and functional improvement in infarcted heart, *J. Cell. Physiol.* 234 (2019) 1671–1681.
- [46] J.-A. Pan, H. Zhang, Q. Yu, J.-F. Zhang, C.-Q. Wang, J. Gu, K. Chen, Association of circulating irisin levels and the characteristics and prognosis of coronary artery disease, *Am. J. Med. Sci.* (2021).
- [47] G. Kong, Y. Jiang, X. Sun, Z. Cao, G. Zhang, Z. Zhao, Y. Zhao, Q. Yu, G. Cheng, Irisin reverses the IL-6 induced epithelial-mesenchymal transition in osteosarcoma cell migration and invasion through the STAT3/Snail signaling pathway, *Oncol. Rep.* 38 (2017) 2647–2656.
- [48] L S, H L, J C, H S, Y Z, F W, W W, W Z, F W, H L, D T, Irisin suppresses the migration, proliferation, and invasion of lung cancer cells via inhibition of epithelial-to-mesenchymal transition, *Biochem. Biophys. Res. Commun.* 485 (2017).
- [49] P. Ježek, B. Holendová, K.D. Garlid, M. Jabůrek, Mitochondrial uncoupling proteins: subtle regulators of cellular redox Signaling Reviewing editors: jerzy beltowski, joseph burgoyne, gabor csanyi, sergey dikalov, frank krause, anibal vercesi, and jeremy ward, *Antioxidants Redox Signal.* 29 (2018) 667–714.
- [50] C. Pecqueur, M.-C. Alves-Guerra, C. Gelly, C. Lévi-Meyrueis, E. Couplan, S. Collins, D. Ricquier, F. Bouillaud, B. Miroux, Uncoupling protein 2, in vivo distribution, induction upon oxidative stress, and evidence for translational regulation*, *J. Biol. Chem.* 276 (2001) 8705–8712.
- [51] J. Huang, W. Peng, Y. Zheng, H. Hao, S. Li, Y. Yao, Y. Ding, J. Zhang, J. Lyu, Q. Zeng, Upregulation of UCP2 expression protects against LPS-induced oxidative stress and apoptosis in cardiomyocytes, *Oxid Med Cell Longev* 2019 (2019) 2758262.
- [52] C. Hu, X. Zhang, W. Wei, N. Zhang, H. Wu, Z. Ma, L. Li, W. Deng, Q. Tang, Matrine attenuates oxidative stress and cardiomyocyte apoptosis in doxorubicin-induced cardiotoxicity via maintaining AMPK α /UCP2 pathway, *Acta Pharm. Sin. B* 9 (2019) 690–701.
- [53] H. Bo, N. Jiang, G. Ma, J. Qu, G. Zhang, D. Cao, L. Wen, S. Liu, L.L. Ji, Y. Zhang, Regulation of mitochondrial uncoupling respiration during exercise in rat heart: role of reactive oxygen species (ROS) and uncoupling protein 2, *Free Radic. Biol. Med.* 44 (2008) 1373–1381.
- [54] K. Chen, Z. Xu, Y. Liu, Z. Wang, Y. Li, X. Xu, C. Chen, T. Xia, Q. Liao, Y. Yao, C. Zeng, D. He, Y. Yang, T. Tan, J. Yi, J. Zhou, H. Zhu, J. Ma, C. Zeng, Irisin protects mitochondria function during pulmonary ischemia/reperfusion injury, *Sci. Transl. Med.* 9 (2017).